

**Strain-path controlled microstructure, texture and hardness evolution
in cryo-deformed AlCoCrFeNi_{2.1} eutectic high entropy alloy**

Amit Patel

A Dissertation Submitted to
Indian Institute of Technology Hyderabad
In Partial Fulfillment of the Requirements for
The Degree of Master of Technology



भारतीय प्रौद्योगिकी संस्थान हैदराबाद
Indian Institute of Technology Hyderabad

Department of Materials Science and Metallurgical Engineering

June, 2018

Declaration

I declare that this written submission represents my ideas in my own words, and where others' ideas or words have been included, I have adequately cited and referenced the original sources. I also declare that I have adhered to all principles of academic honesty and integrity and have not misrepresented or fabricated or falsified any idea/data/fact/source in my submission. I understand that any violation of the above will be a cause for disciplinary action by the Institute and can also evoke penal action from the sources that have thus not been properly cited, or from whom proper permission has not been taken when needed.

Amit Patel

(Signature)

Amit Patel

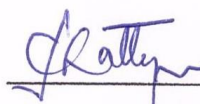
(Student Name)

MS16MTECH11001

(Roll No)

Approval Sheet

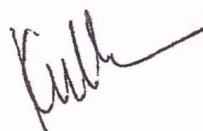
This thesis entitled “Strain-path controlled microstructure, texture and hardness evolution in cryo-deformed AlCoCrFeNi_{2.1} eutectic high entropy alloy” by Amit Patel is approved for the degree of Master of Technology from IIT Hyderabad.



Dr. Subhradeep Chatterjee

Department of Materials Science and Metallurgical Engineering

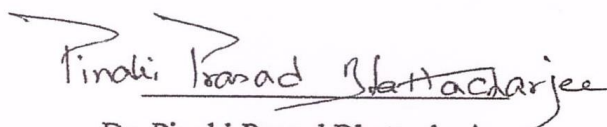
Examiner



Dr. Sairam K Malladi

Department of Materials Science and Metallurgical Engineering

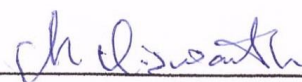
Examiner



Dr. Pinaki Prasad Bhattacharjee

Department of Materials Science and Metallurgical Engineering

Adviser



Dr. Chinthapenta R Viswanath

Department of Mechanical and Aerospace Engineering

Chairman

Acknowledgements

First of all, I would like to express my sincere gratitude to my supervisor **Dr.Pinaki Prasad Bhattacharjee** for giving me an opportunity to work under him on this field. His advice and guidance throughout this work has been of immeasurable help not only in research work, but also in my development as a whole.

I would like to thank Dr. Sheng Guo, from the department of Material and Manufacturing, Industrial and Materials science, Chalmers University of Technology, Sweden for providing the starting material for our work.

I would like to thank Dr. Bharat Bhooshan Panigrahi, Head of the Department for his inspiring word and encouragement towards achieving the goals.

I would also like to thank Mr. S.R.Reddy Mr. Irfan Samad Wani, Mr. N. Swamy, Mr. Veresham Mr. Jaydeep and other research scholars for extending their constant support at every point of time, right from experiments stage till analysis of the results.

I am extremely thankful to Mr. M.V.Srinivas, Mr. B.Raju and other staff members of my department for helping me during whole experimental work.

Finally, I would like to express my deepest gratitude to the Almighty without his blessings, this project would not have been possible.

Abstract

In the present work, the effect of strain-path on the microstructure, texture and hardness properties of AlCoCrFeNi_{2.1} eutectic high entropy alloy was investigated. The EHEA was first cryo-rolled at 77K upto 90% thickness reduction using three different cross-rolling routes namely unidirectional cryo-rolling (UCR), multistep cross-rolling (MSCR) and two-step cross-rolling (TSCR(45°)) followed by annealing at three different temperatures. The UCR processed material showed heterogeneous microstructure as compared to MSCR and TSCR(45°) processed materials. The deformation texture of L1₂/FCC in MSCR processed material agrees quite well the texture of cryo-rolled FCC materials whereas the texture of both the phases in TSCR(45°) processed material appears relatively weak. Upon recrystallization at 800°C, the UCR processed material showed a rather novel heterogeneous microstructure whereas MSCR and TSCR(45°) processed materials indicate ultra-fine micro-duplex structure. At higher annealing temperature, the micro-duplex structures remain stable in all the three processed materials. The annealing texture of L1₂/FCC phase showed presence of strong α -fibre (ND//<110>) whereas B2 phase revealed intense ND-fibre (ND//<111>) which is usual recrystallization texture found in BCC material. The UCR processed material showed much higher hardness as compared to MSCR and TSCR(45°) processed materials which is attributed to its novel heterogeneous microstructure. Hence, it can be concluded that strain-path results in significant influence in controlling microstructure, texture and hardness properties of EHEA.

Nomenclature

HEA- High Entropy Alloy

EHEA- Eutectic High Entropy Alloy

TMP- Thermo-mechanical processing

FCC- Face Centered Cubic

BCC- Body Centered Cubic

HCP- Hexagonal Close Packed

IQ map- Image Quality map

ODF- Orientation Distribution Function

RD- Rolling Direction

TD- Transverse Direction

ND- Normal Direction

UCR-Unidirectional Rolling

MSCR-Multi Step Cross Rolling

TSCR (45°)-Two Step Cross Rolling (45°)

SEM- Scanning Electron Microscopy

LAGB- Low Angle Grain Boundary

EBSD- Electron Back Scattered Diffraction

Bs - Brass orientation

B_S^{ND} - ND rotated Brass orientation

G- Goss orientation

Contents

Declaration	ii
Approval Sheet	iii
Acknowledgements	iv
Abstract.....	v
Nomenclature	vi
1 INTRODUCTION	1
1.1 Overview	1
1.2 Objective of the present work.....	1
2 LITERATURE REVIEW	2
2.1 Eutectic High Entropy Alloys (EHEAs).....	2
2.2 Thermo-mechanical processing of AlCoCrFeNi _{2.1} EHEA.....	2
2.3 Effect of strain-path on microstructure, texture and properties	3
2.4 Novelty of the work.....	4
3 EXPERIMENTAL	5
3.1 Preparation of starting material.....	5
3.2 Processings	6
3.2.1 Cryo-rolling	6
3.2.2 Isochronal Annealing	7
3.3 Characterization	7
4 EXPERIMENTAL RESULTS	8
4.1 Evolution of microstructure and texture during deformation	8
4.2 Evolution of microstructure, texture and hardness during annealing	15
.....	17
5 DISCUSSION	22
5.1 Evolution of deformation microstructure and texture	22
5.2 Evolution of annealed microstructure and texture	24
6 SUMMARY AND CONCLUSIONS.....	26
REFERENCES.....	28

Chapter 1

INTRODUCTION

1.1 Overview

The conventional alloys are based on the concept of one principal element in which other elements are added to enhance the properties of the material. However, with the sharp contrast to this theory, recently the idea of novel multi-components alloys has been introduced in which a large number of elements (usually ≥ 5) are mixed in equiatomic or near equiatomic proportion (5-35 at%) [1]. These are usually known as high entropy alloys (HEAs). Despite their complex concentrated alloy chemistry, the HEAs may show simple crystal structure such as FCC [2], BCC [3], FCC+BCC [4] or even HCP [5]. This is mainly due to an effect of high configurational entropy of mixing which diminishes the free energy and stabilize these simple phases[1]. There are many factors which have considerable effect on the microstructure and properties of HEAs, however, the major contribution comes from the four core effects namely high-entropy, sluggish diffusion, severe lattice distortion and cocktail effects[6-9].

Thermo-mechanical processing (TMP) are now being used as one of the vital method to further enhance the properties of the materials [10, 11]. TMP is a combined process which involves heavy plastic deformation followed by annealing treatment which leads to a significant effect on microstructure, texture and mechanical properties of the material. The effect of usual TMP parameters including plastic strain [12], starting grain size [13], cryo-rolling [14] and heating rate [15] on microstructure and texture development in FCC equiatomic CoCrFeMnNi HEA have been reported.

1.2 Objective of the present work

The present work attempts to understand the effect of strain path on the microstructure, texture and hardness evolution during thermo-mechanical processing of AlCoCrFeNi_{2.1} EHEA. In this experiment, three different cross-rolling routes have been done and the development of microstructure and texture during deformation and annealing has been investigated.

Chapter 2

LITERATURE REVIEW

2.1 Eutectic High Entropy Alloys (EHEAs)

EHEAs are another special subgroup of multiphase HEAs. Guo et al first observed the presence of an eutectic morphology in AlCoCrFeNi_{2.1} EHEA [16]. The EHEAs immediately attracted considerable attention due to their attractive microstructure and possibilities of achieving superior strength-ductility combination. Consequently, the underlying principles for developing EHEAs with novel properties remains a key area of interest.

Although several EHEAs have been reported following the first report by Guo et al [16], the AlCoCrFeNi_{2.1} remains one of the most investigated EHEA system. Guo et al have reported that the eutectic constituent in the is a mixture of FCC and B2 phases. However, Wani et al [10] have established that the as-cast EHEA consisted of an eutectic lamellar mixture of (Ni, Al) rich but Cr depleted B2 phase and Al-depleted L1₂ phases, having volume fractions of ~35% and 65%, respectively. Nanosized precipitates enriched in Cr and having disordered BCC structure are found dispersed inside the B2 phase. Further, the B2 phase reveals dispersion of nano-precipitates having disordered BCC structure [17].

Although the AlCoCrFeNi_{2.1} EHEA shows attractive properties over a temperature range spanning from ambient to cryogenic temperatures [18] even in the as-cast state, thermo-mechanical processing can significantly enhance the properties of the processed materials by controlling microstructure and texture. Hence, understanding the thermo-mechanical processing behavior of EHEAs remains central to developing novel materials for advanced structural applications.

2.2 Thermo-mechanical processing of AlCoCrFeNi_{2.1} EHEA

Wani et al. have extensively investigated the thermo-mechanical processing behavior of AlCoCrFeNi_{2.1} eutectic high entropy alloy (EHEA)[10, 19-21]. The B2 phase is much harder (~ 3 times) than the L1₂ phase as revealed by careful nano-indentation mapping. Heavy cold-rolling to 90% reduction in thickness results in progressive disordering of the L1₂ phase, while the B2 phase remained ordered. Brass type (Bs) deformation texture is observed in the FCC/L1₂ phase, while the B2 phase revealed {111} <110> component located at the intersection of RD (//<110) and ND (//<111>) fibers.

Annealing of the 90% cold-rolled material at 800°C results in a duplex microstructure composed of disordered FCC and precipitate-free B2 phases with equiaxed morphologies and possessing significant resistance to grain growth. Recrystallization texture in L1₂ phase shows the development of α -fiber (ND//<110>) components. The B2 phase shows strong ND fiber (ND//<111>) components. Significant improvement in tensile properties as compared to the as-cast alloy could be achieved by thermo-mechanical processing featured by high tensile strength (≥ 1000 MPa) with tensile ductility over 10%.

Wani et al. have further clarified the remarkable effect of cryo-rolling on microstructure and mechanical properties of the EHEA [22]. The cryo-rolled and annealed EHEA develops a novel heterogeneous microstructure. The heterogeneous microstructure of the cryo-rolled and annealed material results in simultaneous enhancement in strength (Yield Strength/YS: 1437 \pm 26 MPa, Ultimate Tensile Strength/UTS: 1562 \pm 33 MPa) and ductility (elongation to failure/ e_f ~14 \pm 1%) as compared to the as-cast as well as cold-rolled and annealed materials.

2.3 Effect of strain-path on microstructure, texture and properties

In addition to typical thermo-mechanical processing variables, strain-path remains a key parameter having considerable effects on microstructure and properties. The effect of strain-path during deformation can be understood by cross-rolling. In contrast to conventional rolling in which the rolling direction (RD) is maintained constant throughout the processing, the RD is not fixed during cross-rolling. Strain-path leads to continuous destabilization of the deformed substructure in the cross-rolled materials which substantially affect the texture of the various metals and alloys [23-25].

The effect of strain-path on microstructure and texture in single FCC phase CoCrFeMnNi HEA has been investigated by Reddy et al [26]. The alloy could be processed through three different cross-rolling routes. In unidirectional cold-rolling (UCR), the rolling direction (RD) is kept unchanged throughout the processing. In multistep cross-rolling (MSCR), the sheets are rotated by 90° about the normal direction (ND) after each pass, so that the RD and the transverse direction (TD) are interchanged in every pass. In the two step cross cold-rolling (TSCR) route, the samples are first deformed to half of the total equivalent strain ($\epsilon_{eq}/2 \sim 1.3$ corresponding to a thickness reduction of ~65%) along a fixed RD. Further thickness reduction to total equivalent strain of ~2.65 (corresponding to 90% reduction in thickness) is carried out using two different routes. In the TSCCR(90°) route, the samples are rotated by 90° around ND and the further rolling was carried out along the new direction. In

the TSCCR(45°) route, the sample are rotated by 45° around ND and further deformation was carried along this diagonal direction. Therefore, the direction of rolling is changed only once (i.e. after stage 1 after a true equivalent strain of ~1.3) in the TSCCR(90°) and TSCCR(45°) routes [26].

The TSCCR(45°) processed material appears to develop shear bands. The UCR processed material shows brass type texture, while the textures of different cross-rolled materials are featured by different rotated brass components. Upon annealing, the UCR processed material shows the lowest grain size while the highest grain size is observed in the TSCCR(45°) processed material. This indicates greater availability of nucleation sites in the UCR processed material as compared to the TSCCR(45°) processed material. The differences in annealed grain size could be attributed to substructure destabilization and misorientation build-up, thus diminishing the number of potential nuclei in the TSCCR(45°) processed material. The annealing textures of the differently processed materials are featured by the presence of α -fiber (ND// $\langle 110 \rangle$) and absence of preferential nucleation and growth [26].

Strain-path exerts a significant influence on mechanical properties such as hardness. It was pointed out that the cross-rolled products shows higher hardness value as compared to conventional UCR processed material in HCP metals like Ti [27]. However, in some cases, the UCR processed materials show lower hardness as compared to different cross-rolled samples [28]. These conflicting reports indicate that the effect of strain path on mechanical behavior of materials needs to be understood in depth.

2.4 Novelty of the work

In the present work, the effect of strain-path on microstructure, texture, and hardness in AlCoCrFeNi_{2.1} eutectic high entropy alloy (EHEA) processed by heavy cryo-rolling is investigated for the first time. As already highlighted, cryo-rolling exerts significant influence on microstructure and mechanical properties of EHEAs [29, 30]. Therefore, further tailoring and enhancing properties through strain-path remain distinct possibilities. These unexplored issues remain the major motivation for undertaking the present research.

Chapter 3

EXPERIMENTAL

3.1 Preparation of starting material

AlCoCrFeNi_{2,1} EHEA was used as a starting material in the present work. The EHEA was prepared by arc melting in a Ti-gettered high-purity argon atmosphere with high purity (>99.9%) starting materials. Once the molten alloy was cast into the copper mold, rectangular specimens of dimensions 20 mm (long) × 15 mm (wide) × 3 mm (thick) were cut from the as-cast EHEA. The surface of the as-cast slabs were carefully polished to remove any contamination. The schematic representation of the present work in the form of flow chart is shown in Fig.3.1.

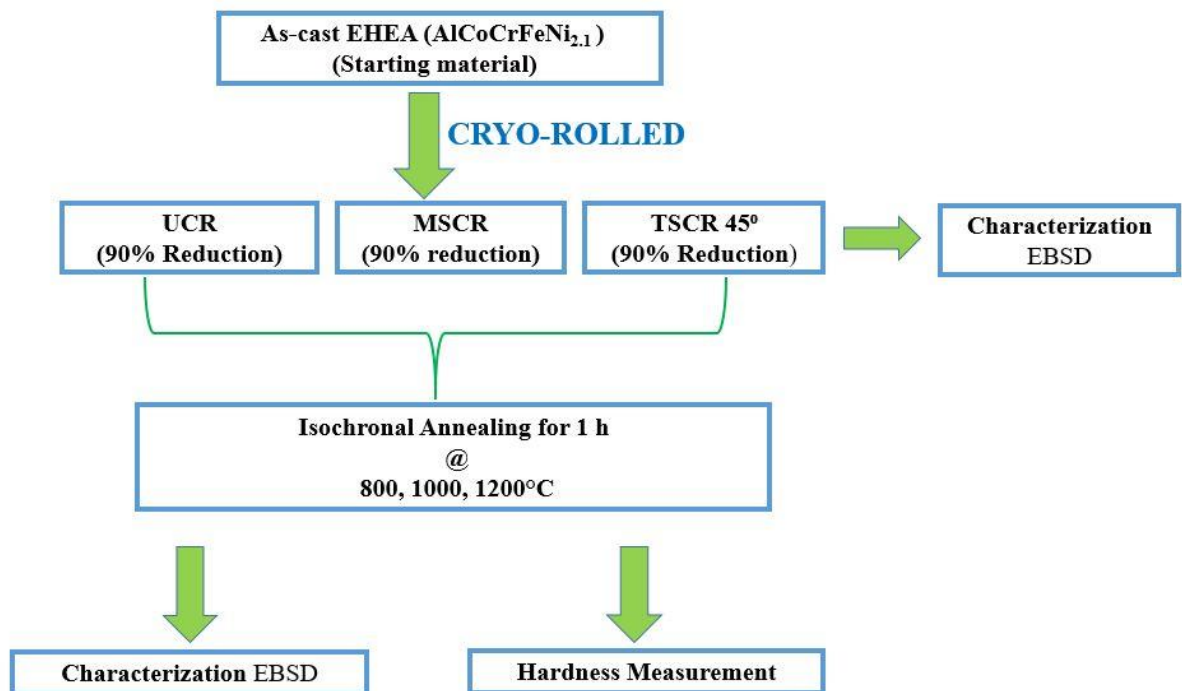


Fig.3.1 Experimental flow chart of the present work

3.2 Processings

3.2.1 Cryo-rolling

The EHEA samples were deformed up to 90% reduction using different multistep cross-rolling routes as shown in fig.3.2. During unidirectional cryo-rolling (UCR) (Fig.3.2(a)), the rolling direction (RD) was fixed until 90% deformation (corresponding to equivalent strain of 2.65). In multistep cross-rolling (MSCR) (Fig.3.2(b)), the samples were rotated by 90° about the normal direction (ND) after each pass. This obviously resulted in mutual interchange of RD and transverse direction (TD) in each pass. In two-step cross-rolling (TSCR 45°) (Fig.3.2(c)), the samples were first deformed up to 65% reduction unidirectionally up to half of the equivalent strain ($\epsilon \sim 1.3$), and then the rest of the deformation up to 90% was imparted by rolling along the direction inclined 45° to the original RD. In all the three different modes of cross-rolling, the samples were immersed in the liquid N₂ for 30 minutes before and immediately after each rolling pass.

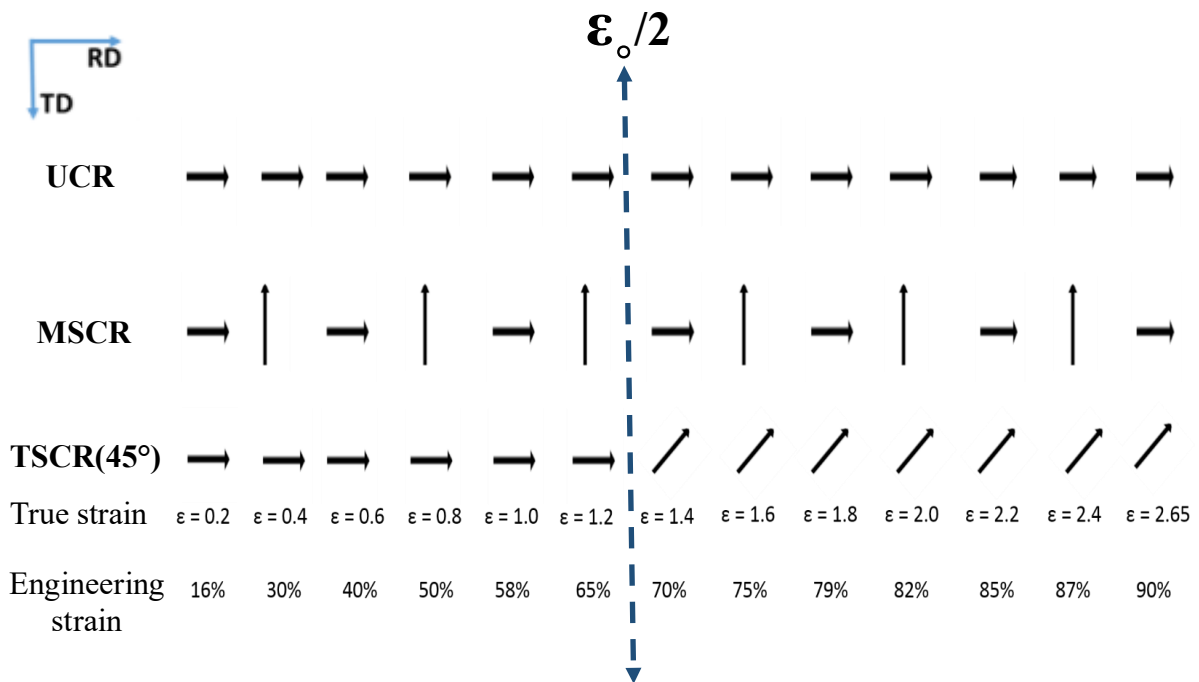


Fig.3.2 Schematic showing (a) UCR (b)MSCR (c) TSCR (45°) processing routes.

3.2.2 Isochronal Annealing

In order to study the effect of strain-path on the microstructure and texture evolution, small samples obtained from the 90% cryo-rolled sheets were subjected to isochronal annealing treatments for 1 hr at three different temperatures, namely 800°C, 1000°C, and 1200°C respectively. The annealed samples were immediately quenched in cold water following the heat treatments.

3.3 Characterization

The microstructure and texture of the cryo-deformed and annealed samples prepared using different strain-paths were investigated using electron backscattered diffraction (EBSD) system (Oxford Instruments, UK) attached to a FEG-SEM (Maker: Carl-Zeiss, Germany; Model: Supra 40). The acquired EBSD data were analyzed by TSL-OIM™ (EDAX, USA) software.

Since 90% deformed samples were having many unindexed regions, so phase fractions in the deformed EHEA processed by the different cross-rolling routes were calculated from the SEM micrographs using the ImageJ software [31]. The deformed and annealed samples were mechanically polished using colloidal silica followed by electro-polishing using a mixture of perchloric acid and methanol in a ratio of 1:9 (by volume) at 0° C temperature. Several EBSD scans were taken from different regions of each deformed and annealed samples. The scans were merged for the calculation of the orientation distribution functions (ODFs). The ODFs were calculated using the series expansion method with series rank 22.

Chapter 4

EXPERIMENTAL RESULTS

4.1 Evolution of microstructure and texture during deformation

The SEM micrographs of the 90% cryo-deformed materials processed by different routes are shown in the Fig.4.1. In the UCR processed material (Fig.4.1(a)), the microstructure reveals lamellar regions (marked by yellow circles) elongated along the RD co-existing with fine fragmented regions (shown by white circles). In contrast, the SEM micrographs of the MSCR (Fig.4.1(b)) and TSCR(45°) (Fig.4.1(c)) processed materials show remarkably fragmented B2 phase. These fragmented B2 phases are having elongated and spherical morphologies. The elongated B2 phase is several microns in length, whereas fragmented B2 phase shows a wider range in size.

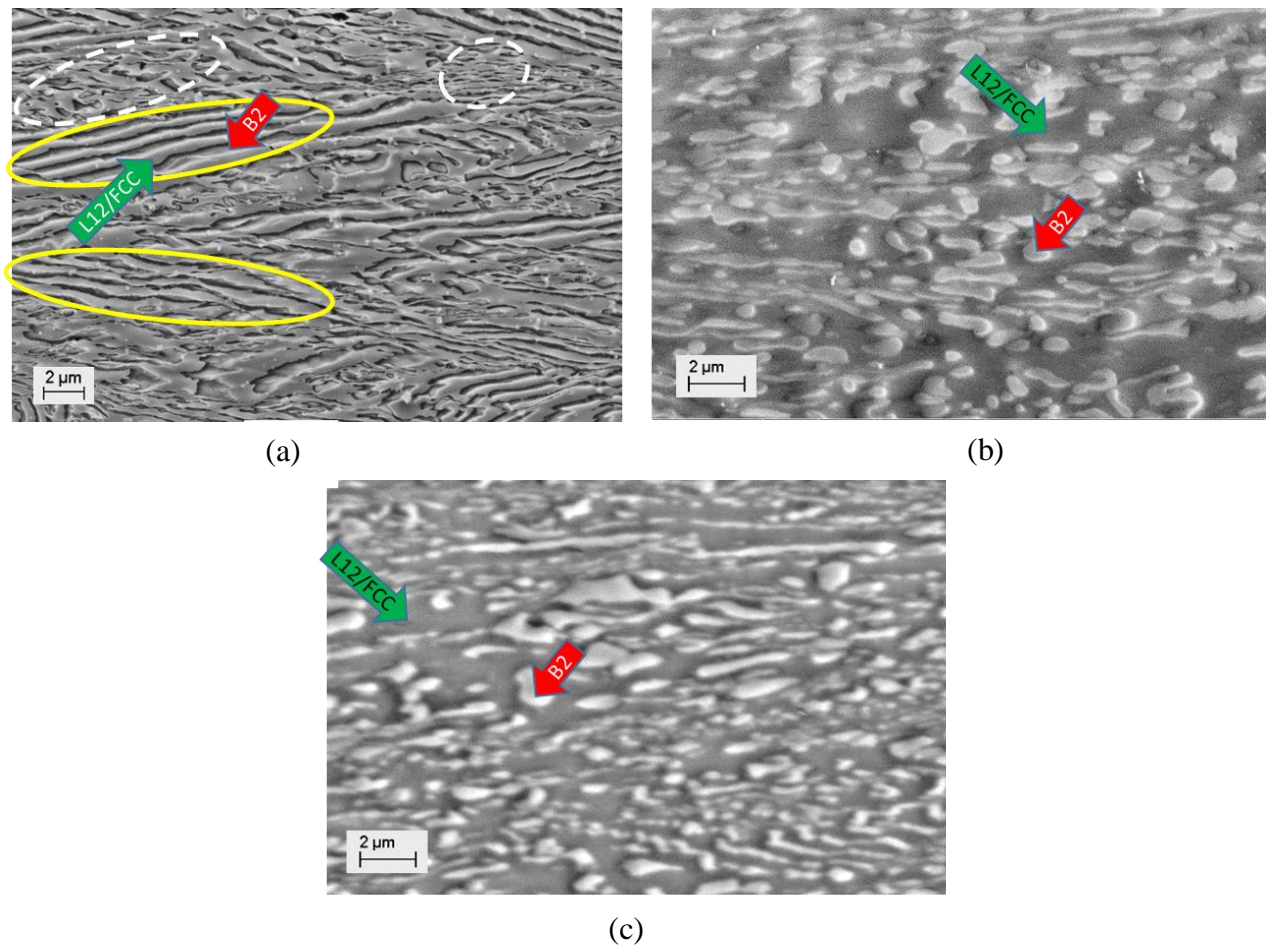
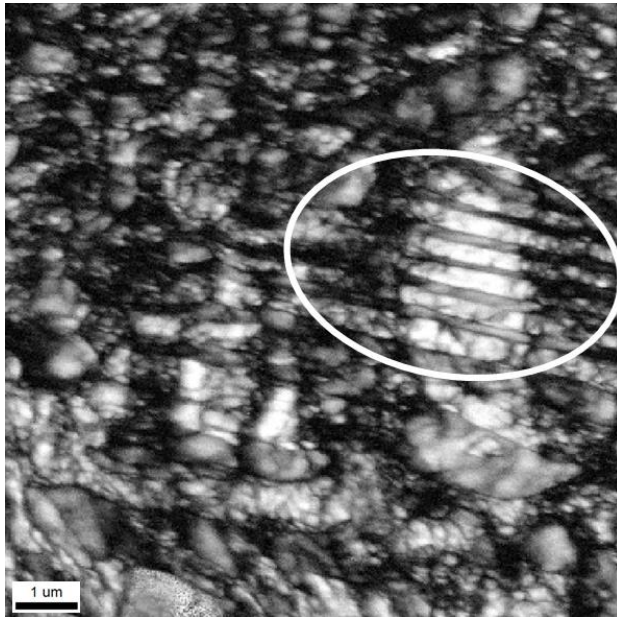


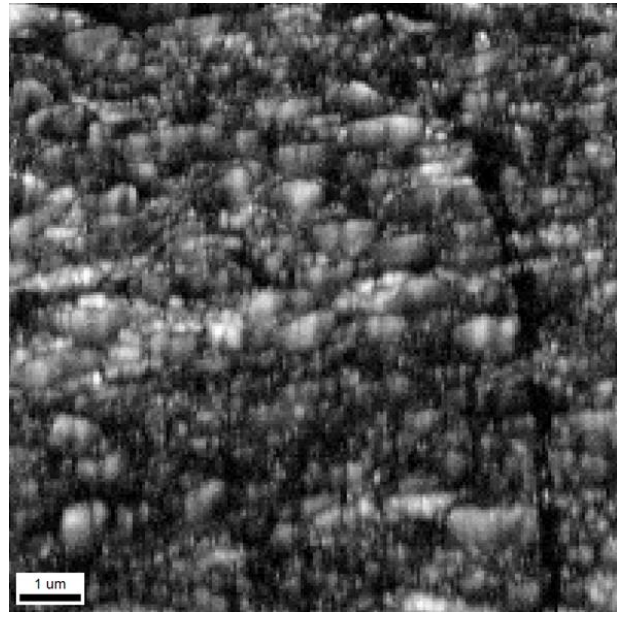
Fig.4.1: SEM micrographs of 90% cryo-rolled EHEA processed by (a) UCR, (b) MSCR and (c) TSCR(45°) processing routes

The remarkable differences in the microstructure of the three processed materials can be understood from the EBSD image quality maps (IQ) (Fig.4.2). The IQ map of the UCR processed materials (Fig.4.2(a)) shows heterogeneous microstructure having a narrow lamellar region (marked by circle) along with fine fragmented regions. However, the IQ maps of the MSCR (Fig.4.2(b)) and TSCR (45°) (Fig.4.2(c)) processed materials depicts severely fragmented microstructure such that lamellar eutectic regions are not observed unlike UCR processed material.

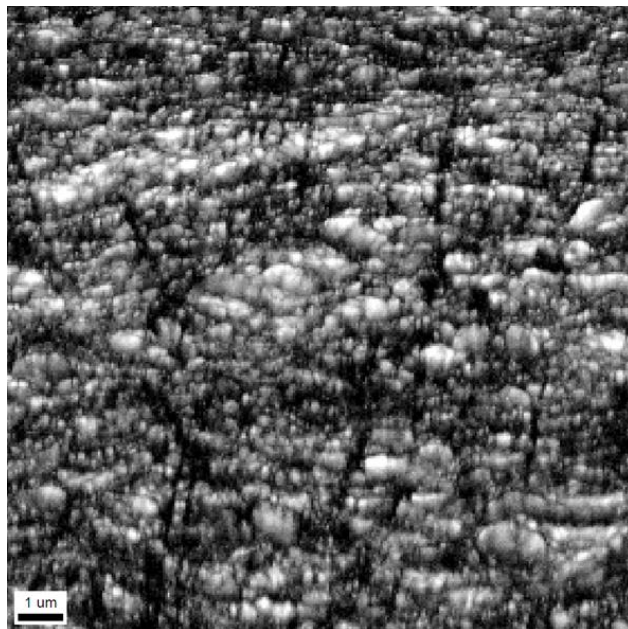
The phase fraction of the constituent $L1_2$ /FCC and B2 phases of 90% cryo-rolled EHEA processed by three different routes are compared in Fig.4.3. The phase fraction (calculated using Image J software) doesn't show much variations in all the three processed material including as-cast EHEA.



(a)



(b)



(c)

Fig.4.2: EBSD IQ maps of 90% cryo-rolled EHEA processed by (a) UCR, (b) MSCR and (c) TSCR (45°) processing route

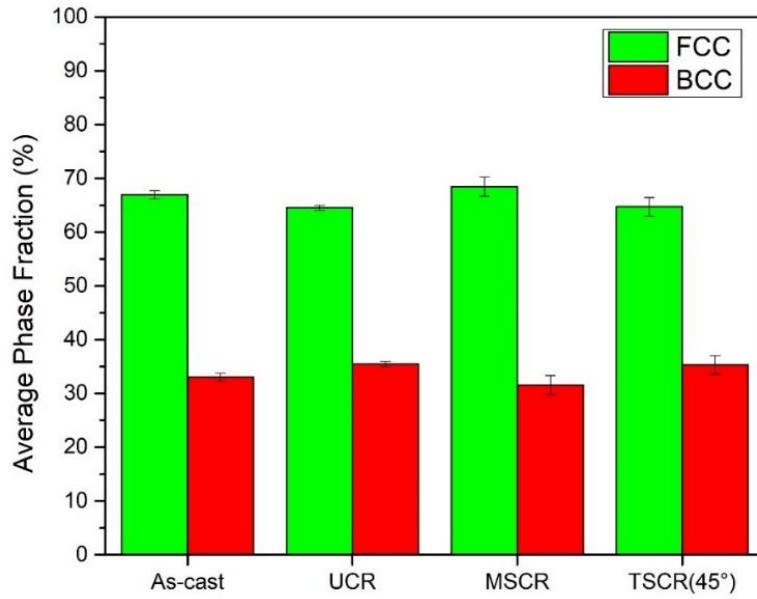


Fig.4.3: Phase fraction in as-cast and 90% cryo-deformed EHEA processed by different rolling routes.

Table 1: List of important deformation and recrystallization texture components in $L1_2$ /FCC phase

Texture component	Symbol	Euler angle (°)			Miller Indices
		Φ_1	Φ	Φ_2	
Cube (C)	■	0, 0, 0			{001} <100>
Copper (Cu)	●	90,35,45			{112}[4] <111>
S	▲	59,37,63			{123} <634>
B _s	▼	35,45,0			{110} <112>
G	◆	0,45,0			{110} <001>
Rt-G	★	90,45,0			{110} <110>
G/B	◄	17,45,0			{110} <115>
B _s /B _s ND	●	45,45,0			{110} <755>
B _s ND	▶	55,45,0			{110} <111>
BR	⬡	80,31,34			{236} <385>
D	⌘	90,25,45			{113} <332>
K	⊗	27,64,14			{142} <211>
M	⊗	80,30,65			{13 6 25} <20 15 14>

The development of texture in the L1₂/FCC phase of the 90% cryo-deformed material processed by the three different routes is shown by the relevant ODF sections in Fig.4.4. The important deformation and recrystallization texture components in the L1₂/FCC phase of the HEAs are summarized in Table 1. In the UCR processed material(Fig.4.4(a)), the $\varphi_2 = 0^\circ$ section of the ODF of the L1₂/FCC phase shows strong intensity at $\varphi_1, \Phi, \varphi_2 = (25^\circ, 45^\circ, 0^\circ)$ between G and B_s texture components, but somehow shifted from ideal B_s location. The $\varphi_2 = 45^\circ$ section of the ODF reveals the presence of the Cu component whereas the $\varphi_2 = 65^\circ$ section confirms the S component which is rather weak. In contrast, the $\varphi_2 = 0^\circ$ section of the ODF in the MSCR processed material (Fig.4.4(b)) shows the development of an α -fiber (ND// <110>) having strong intensity at G and exactly at the $\varphi_1, \Phi, \varphi_2 = (45^\circ, 45^\circ, 0^\circ)$ location corresponding to the B_s/BSND component {011}<755>. The $\varphi_2 = 45^\circ$ section of the ODF shows a complete absence of Cu-component. In TSCR(45°) (Fig.4.4(c)) processed material, the $\varphi_2 = 0^\circ$ section only shows intensities at the vicinity of the G orientation but does not show {011}<755> texture component unlike the MSCR processed material. Presence of an (011)[122] orientation corresponding to $\varphi_1, \Phi, \varphi_2 = (66^\circ, 45^\circ, 0^\circ)$ along the α -fiber is also noticed. However, the $\varphi_2 = 45^\circ$ section confirms the complete absence of Cu component in this case as well.

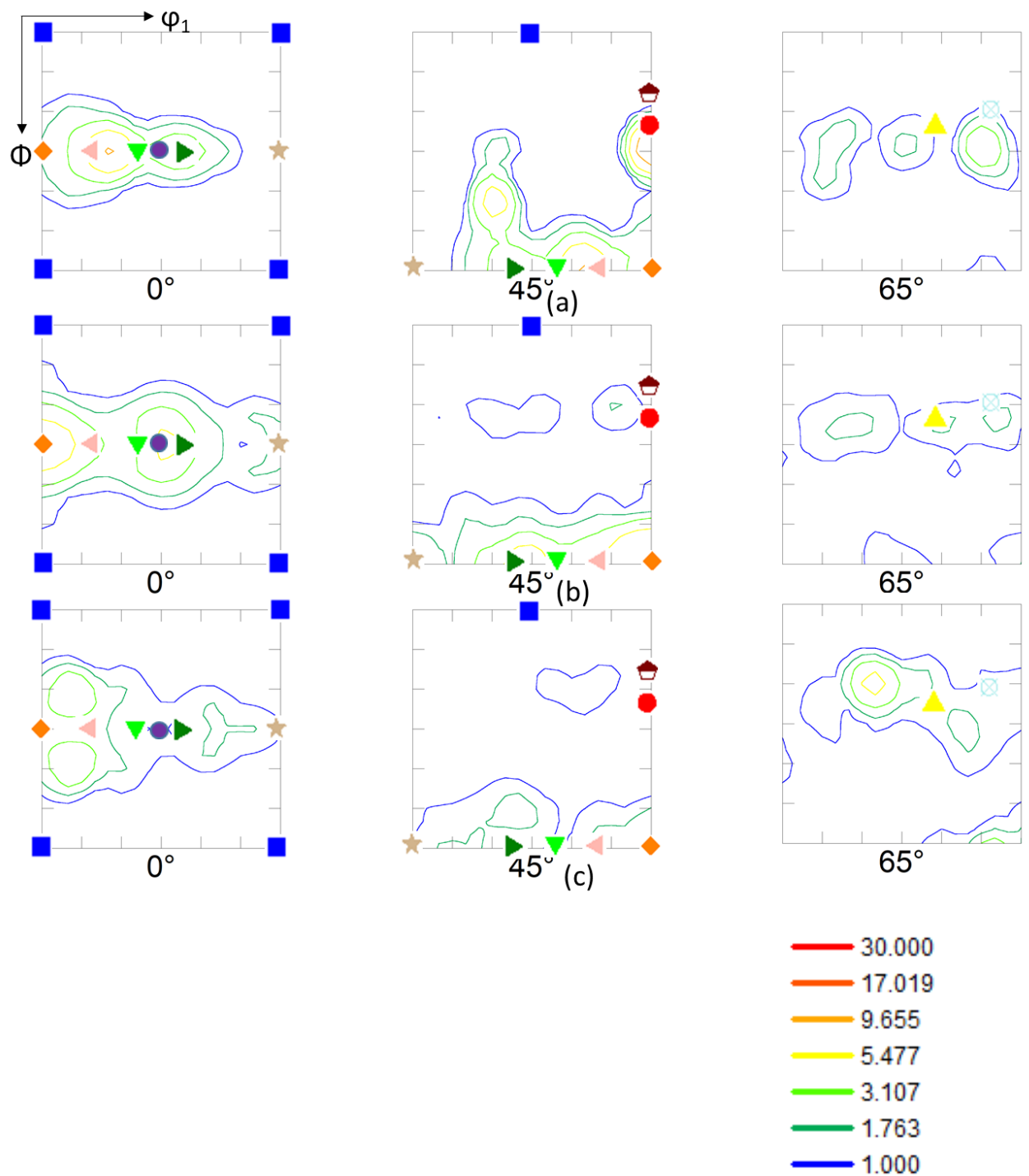







Fig.4.4: Relevant ODF sections of the $L1_2$ /FCC phase in 90% cryo-rolled EHEA processed by (a) UCR, (b) MSCR and (c) TSCR(45°) processing routes (for legends, refer to Table 1).

Table 2: List of Important deformation and recrystallization texture components in the B2 phase.

Texture component	Symbol
$\{001\}\langle 110\rangle$	
$\{114\}\langle 110\rangle$	
$\{112\}\langle 110\rangle$	
$\{111\}\langle 110\rangle$	
$\{111\}\langle 112\rangle$	

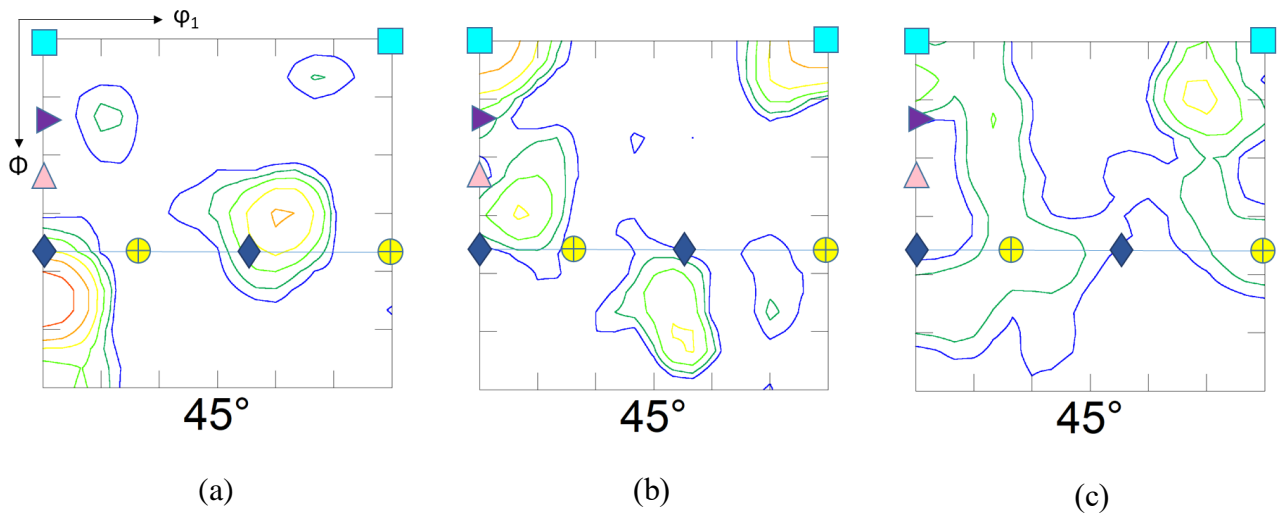


Fig.4.5: $\phi_2=45^\circ$ section ODFs of the B2 phase in 90% cryo-rolled EHEA processed by (a) UCR, (b) MSCR and (c) TSCR(45°) processing routes (for legends, refer to Table 2). The intensities of the contour lines are same as in Fig.4.4

The texture of B2 phase in the 90% cryo-rolled materials processed by three different processed routes is shown in Fig.4.5. The important texture components in the B2 phase of the HEAs are summarized in Table 2. The $\phi_2=45^\circ$ section of the ODF of the B2 phase in the UCR processed material (Fig.4.5(a)) shows slightly shifted $\{111\}\langle 011\rangle$ component which lies at the intersection of the ND and RD-fibers. In contrast, the $\phi_2=45^\circ$ section of the ODF of the B2 phase in the 90% MSCR processed material (Fig.4.5(b)) shows a distinct $\{001\}\langle 110\rangle$ component belonging to the RD-fiber. The intensities of the contour lines show that the texture is weakened after MSCR processing. In the 90% TSCR(45°) processed material (Fig.4.5(c)), the $\phi_2=45^\circ$ section of the ODF shows the absence of any predominant RD or ND-fiber components. The texture appears to be significantly weakened in this case. In essence, the texture is weakened in both MSCR and TSCR(45°) processed materials.

4.2 Evolution of microstructure, texture and hardness during annealing

The development of microstructure in the 90% deformed material after annealing is shown in Fig.4.6. The phase map of the UCR processed material after annealing at 800°C (Fig.4.6(a)) shows a remarkable heterogeneous microstructure characterized by lamellar regions and non-lamellar regions of coarse B2 and ultra-fine recrystallized $L1_2/\text{FCC}$ grains. The coarse B2 phase shows extensive LAGB network (highlighted by white lines) indicating that the B2 grains are still in unrecrystallized condition. However, after annealing at 1000°C (Fig.4.6(b)) and 1200°C (Fig.4.6(c)), the heterogeneous microstructure is replaced by relatively homogeneous fine micro-duplex structure. In stark contrast MSCR (Fig.4.6(d)) and TSCR(45°) (Fig.4.6(g)) processed material show the development of micro-duplex structure after annealing at 800°C unlike the UCR processed material. The micro-duplex structure is rather stable even after annealing at 1000°C and 1200°C in both these cases.

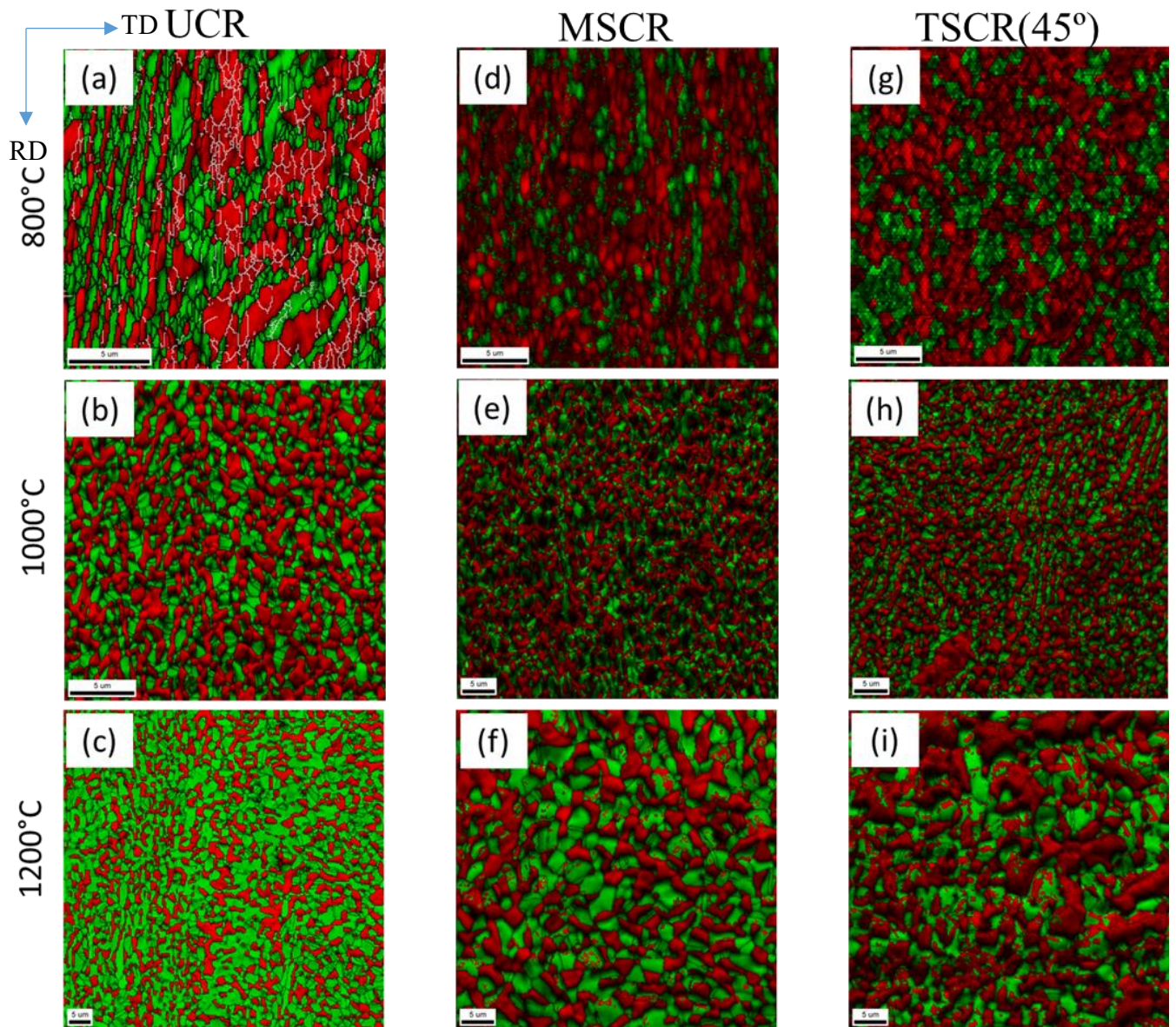


Fig.4.6: EBSD phase map of EHEA processed by ((a)-(c)) UCR, ((d)-(f)) MSCR and ((g)-(i)) TSCR(45°) following annealing at ((a), (d), (g)) 800°C, ((b), (e), (h)) 1000°C and ((c), (f), (i)) 1200°C

The change in FCC phase fraction with annealing temperature in the EHEA processed by the three different routes are compared in Fig.4.7(a). In the 90% cryo-deformed state, the materials processed by the three different routes shows very similar phase fractions. The L₁₂/FCC phase fraction decreases in all the three processed materials after annealing at 800°C. It has been observed that the decrease in the L₁₂/FCC phase fraction is relatively lower in the UCR processed material as compared to the EHEA processed by the other two routes. The L₁₂/FCC phase fraction tends to increase in all the three processed materials with increasing annealing temperature. However, the UCR processed material show higher L₁₂/FCC phase fraction after annealing at 1200°C as compared to the MSCR and TSCR(45°) processed materials.

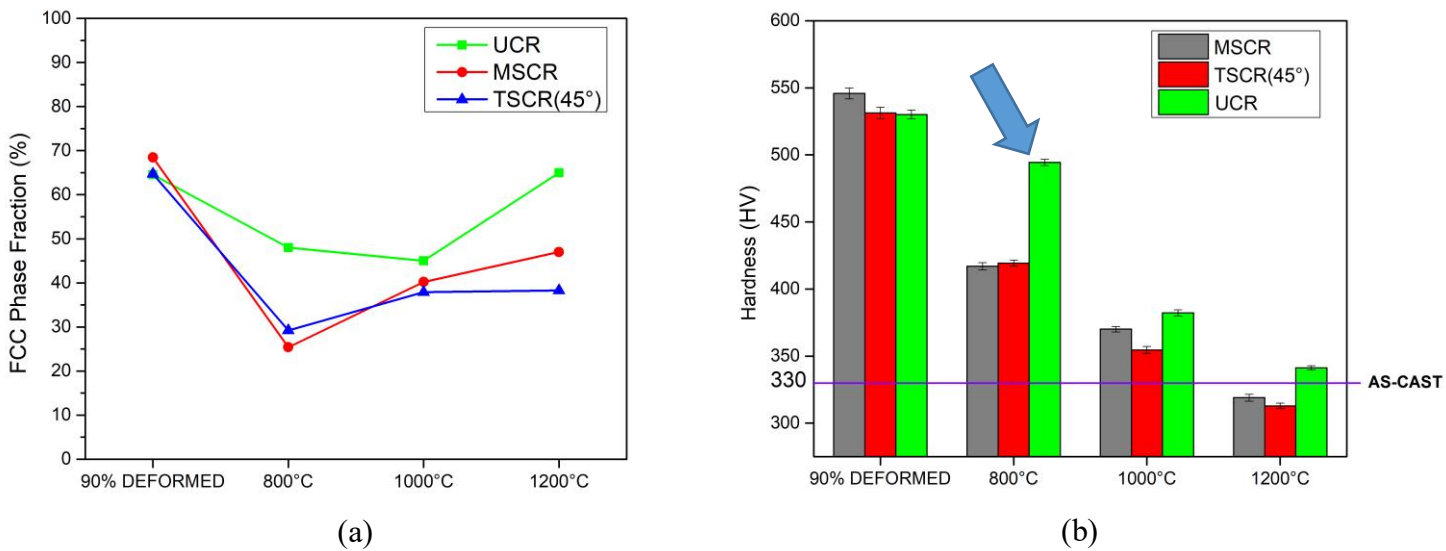


Fig.4.7: (a) Change in phase fraction and (b) hardness with annealing temperature in the EHEA processed by the three different routes.

The evolution of hardness in the materials processed with three different routes reveals very interesting behavior (Fig.4.7(b)). The hardness of the EHEA increases significantly after cryo-rolling by three processed routes as compared to as-cast material. However, the hardness value is quite similar in all the three processed material after 90% cryo-deformation. Remarkably, the hardness value of the UCR processed material is much greater than the those of MSCR and TSCR(45°) processed materials after annealing at 800°C. Following annealing at 1000°C and 1200°C, the EHEA processed by the three different routes again shows very similar hardness values.

The evolution of texture in the $L1_2$ /FCC phase of the annealed EHEA are summarized in Fig.4.8. The $\varphi_2 = 0^\circ$ section are shown to highlight the major changes in texture. The $\varphi_2 = 0^\circ$ section of the ODF of the UCR processed material annealed at 800°C (Fig.4.8(a)) shows intensity at the vicinity of G component. The G component is strengthened with increasing annealing temperature (Fig.4.8(b)), however, upon further annealing at 1200°C, the G/B component emerge as the strongest recrystallization texture component (Fig.4.8(c)). In contrast, the MSCR processed sample annealed at 800°C (Fig.4.8(d)) appears to develop an α -fiber containing $\{011\}\langle 755 \rangle$ component. The $\{011\}\langle 755 \rangle$ component is strengthened with increasing annealing temperature (Fig.4.8(e) and (f)). The TSCR(45°) processed sample also shows the development of a weak α -fiber after annealing at 800°C (Fig.4.8(g)). With increasing annealing temperature, the intensity spreading between B_s and B_s^{ND} is particularly high ((Fig. 4.8(h) and (i)). The material annealed at 1200°C shows a strong intensity at the $\{011\}\langle 755 \rangle$ location (Fig. 4.8(i)).

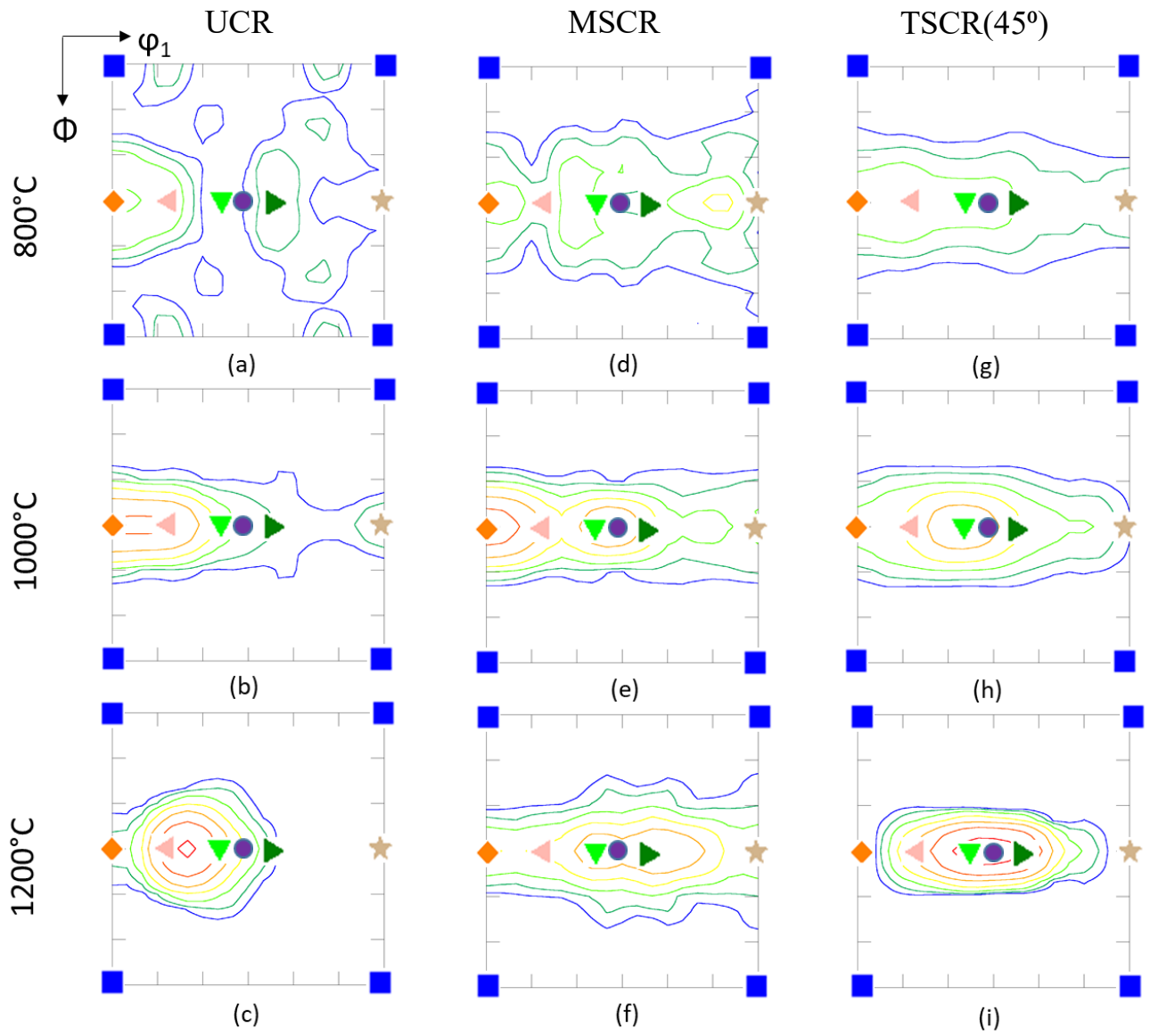


Fig.4.8: $\phi_2=0^\circ$ ODF sections of the $L1_2/FCC$ phase in annealed EHEA processed by different routes (for legends, refer to Table 1). The intensities of the contour lines are same as in Fig.4.4.

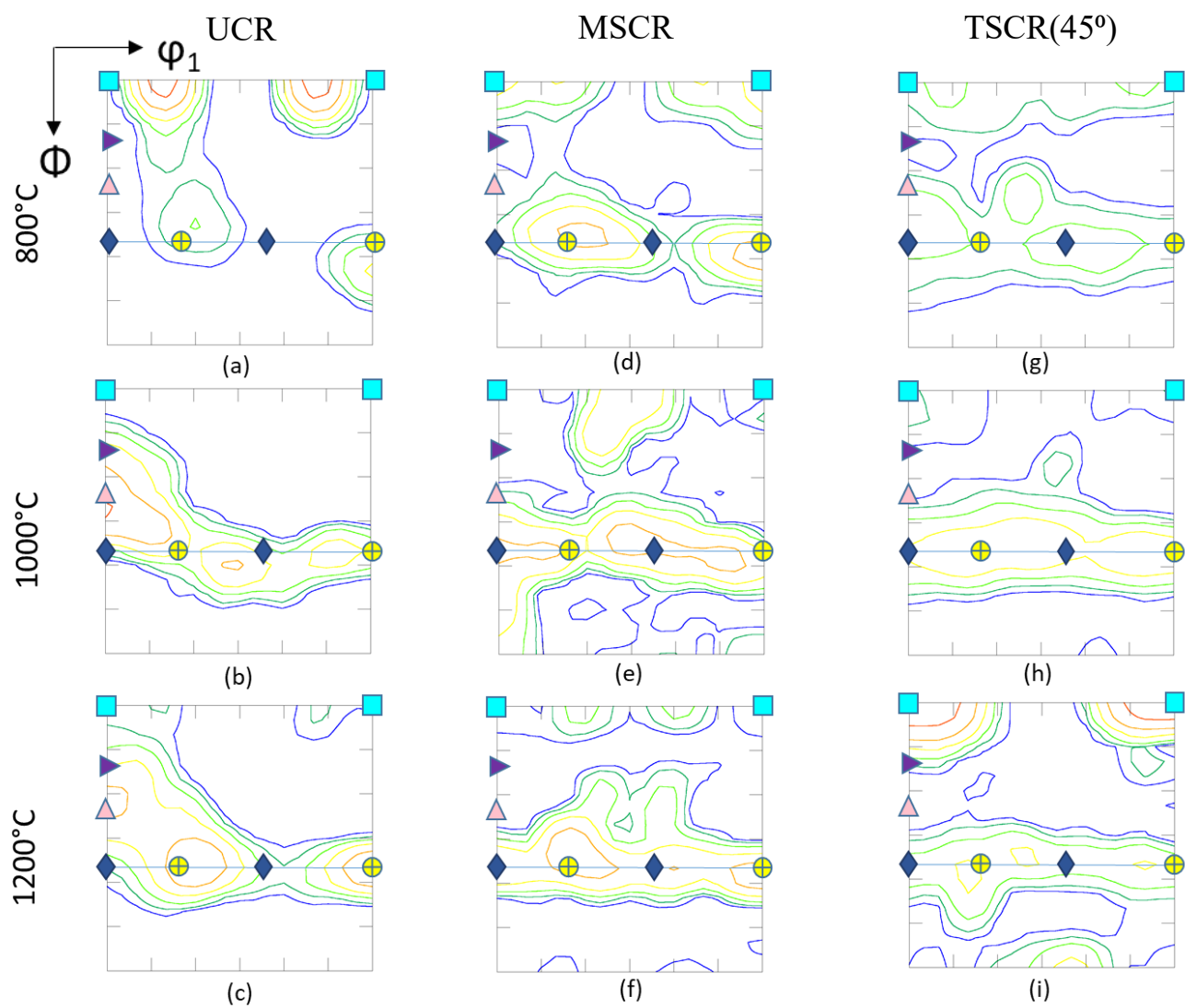


Fig.4.9: $\phi_2=45^\circ$ section of the ODFs of the B2 phase in annealed EHEA processed by different route (for legends, refer to Table 2). The intensities of the contour lines are same as in Fig.4.4.

The evolution of texture in the B2 phase is summarized in Fig.4.9. The $\phi_2 = 45^\circ$ section of the ODF of the UCR processed material annealed at 800°C (Fig.4.9(a)) shows presence of rotated cube components. However, after annealing at 1000°C (Fig.4.9(b)), the ODF of the B2 phase shows the presence of usual RD and ND components. The ODF section in the 1200°C annealed material reveals very similar texture to that of the 1000°C material confirming no significant change in texture at higher temperature. In case of MSCR processed material, the $\{001\}\langle 110\rangle$ component present in the deformed condition in the MSCR processed material persists even after annealing at 800°C (Fig.4.9(d)) along with a strong ND-fiber. The ND-fiber is strengthened with increasing annealing temperature (Fig.4.9(e) and (f)). The texture of the B2 phase in the TSCR (45°) material is rather weak in the 800 °C annealed condition (Fig.4.9(g)), however, formation of a strong ND-fiber is also observed in this case after annealing at 1000 °C (Fig. 4.9(h)) and 1200°C (Fig. 4.9(i)).

Chapter 5

DISCUSSION

5.1 Evolution of deformation microstructure and texture

The analysis of phase fraction in 90% cryo-deformed EHEA processed by the different rolling routes including as-cast material show no significant differences. This clearly indicates that the evolution of microstructure and texture in the three processed materials is not affected by phase transformations. The SEM micrograph and EBSD IQ map of the UCR processed material show the retention of the lamellar regions inherited from the as cast microstructure of the EHEA along with the fine fragmented B2 phase. In contrast, MSCR and TSCR(45°) processed materials reveal severe fragmentation of the B2 phase. The observed differences in microstructures could be rationalized considering the behavior of the two constituent phases. The careful nano-indentation mapping of the as-cast EHEA shows that the B2 phase is much harder than the L1₂/FCC phase [21]. Consequently, during heavy cold-rolling, the softer L1₂/FCC phase is deformed to a much larger extent as compared to the harder B2 phase which is rather easily fragmented. Thus, the microstructure of the EHEA heavily cold-rolled by the UCR route at room temperature shows the formation of deformation induced ultrafine to nanocrystalline grains FCC phase but presence of the mechanically fragmented B2 phase. At the cryo-rolling temperature, the B2 phase is expected to be even harder than the L1₂/FCC phase, which should lead to more strain partitioning to the L1₂ phase. Thus, the fragmentation of the B2 phase is observed in the EHEA processed by all the three rolling routes. Since the rolling direction is maintained constant in the UCR processing route, the starting lamellar microstructure is not completely destroyed, so that the deformed microstructure shows the retention of the lamellar regions inherited from the as cast microstructure of the EHEA. However, structural rotation due to change in strain path in the MSCR and TSCR(45°) processing routes results in a complete fragmentation of the microstructure.

The genesis of deformation texture is correlated with the relative stability of different orientations through the rotation field $\dot{R}(\varphi_1, \varphi, \varphi_2)$ and the divergence of the rotation field $(div \dot{R} = \frac{\partial \varphi_1}{\partial \varphi_1} + \frac{\partial \varphi}{\partial \varphi} + \frac{\partial \varphi_2}{\partial \varphi_2})$ [32] [33]. For a stable orientation: $\dot{R} = 0$ and $div(\dot{R}) = 0$. Hong et al [34] have shown that the orientation $\{011\} \langle 111 \rangle$ (which is basically ND rotated B_s or B_sND orientation lying on the α -fiber corresponding to $\varphi_1, \Phi, \varphi_2 = (55^\circ, 45^\circ, 0^\circ)$) would be stable

under cross-rolling due to its higher inverse rotation rate and large negative divergence. Thus, the α -fiber orientations will converge at the B_s orientation (stable orientation during unidirectional rolling) and then will further rotate away to the $\{011\}\langle 111\rangle$ orientation when the RD is rotated by 90° . Thus, the orientations will be oscillating between the B_s and B_s^{ND} ($\{011\}\langle 111\rangle$), converging at $\varphi_1, \Phi, \varphi_2 = (45^\circ, 45^\circ, 0^\circ)$ corresponding to the orientation $\{011\}\langle 755\rangle$ (B_s/B_s^{ND}) lying at the middle of the two dynamically stable end orientations B_s and B_s^{ND} .

The deformation texture of the $L1_2$ /FCC phase in the UCR processed material shows clear presence of the B_s component. In contrast, the MSCR processed material shows the development of α -fiber with a strong intensity peak exactly at the B_s/B_s^{ND} or the $(011)[755]$ location. Evidently, the deformation texture of the $L1_2$ /FCC phase agrees quite well with the theoretical calculations of Hong et al. [34] and also with the cross-rolling texture of different FCC materials [23]. On the other hand, the $L1_2$ /FCC phase in the material processed by the TSCR(45°) route shows a G/B component and $(011)[122]$ component lying on the α -fiber, which is different from the $\{011\}\langle 755\rangle$ component predicted by Hong et al. [34]. Applying the analogy of Hong et al. [34] for predicting the origin of $\{011\}\langle 755\rangle$ component in MSCR processed material, simple rotation of the B_s component by 45° does not lead to the observed components in the TSCR(45°) material. A very similar behavior is observed for TSCR(45°) processed equiatomic CoCrFeMnNi HEA [26]. This argument has been further supported by the study on diagonally rolled Cu (45° rolling to the prior RD similar to the TSCCR(45°) route, but the strain in step 1 and step 2 are different than in the present study) which develops different texture than 90° cross-rolled materials [35].

The B2 phase in the UCR processed material shows a strong but slightly shifted $\{111\}\langle 011\rangle$ component which has been reported for some cold-rolled B2 phases. The MSCR processed material shows a distinct $\{001\}\langle 110\rangle$ component which is typically observed in cross-rolled BCC, such as ferrite in duplex steel [36] and can be followed from the stability analysis of deformation texture components in BCC materials. In contrast, the B2 phase in the TSCR(45°) shows rather weak texture. Thus, the textures of both FCC and B2 phases are significantly different in the TSCR(45°) processed EHEA. It appears that a 45° rotation around the RD can affect the deformation and slip activities more fundamentally, leading to the observed differences in texture.

5.2 Evolution of annealed microstructure and texture

The EHEA processed by the UCR route shows remarkably heterogeneous microstructure comprising of fine lamellar and coarse non-lamellar regions after annealing at 800°C, while the MSCR and TSCR(45°) processed materials show rather homogeneous microduplex structure. The fine lamellar regions observed in the annealed microstructure of the UCR processed material are already present in the deformed microstructure. Further, due to the deformation carried out at the cryo-rolling temperature, the strain is mostly partitioned to the softer FCC phase as compared to the harder B2 phase. Consequently, the rather small accumulated strain in the B2 phase leads to insignificant driving force for recrystallization. Thus, the B2 phase undergoes recovery which is evidenced by the presence of heavy LAGB network inside the grains, while the severely deformed FCC phase gives rise to ultrafine recrystallized grains. Upon annealing at higher temperatures, the lamellar regions in the UCR processed material are completely broken down to yield microduplex structure. In contrast, the strain-path change implemented in the MSCR and TSCR(45°) processing routes results in a severely fragmented microstructure. Upon recrystallization, the fragmented deformed microstructures lead to fine microduplex structure. Thus, the annealed microstructure in the three processed material could be adequately explained on the basis of characteristics differences in the deformed microstructures.

In all the three processed materials, the FCC phase fraction decreases after annealing at 800°C but increases with increasing annealing temperature, indicating that the FCC phase becomes stable at higher annealing temperature. This trend is observed in cold-rolled EHEA [19] and also in dual phase HEAs, such as Al_{0.5}CoCrFeMnNi [4] , and could be understood from the fact that the phase fractions in duplex materials vary depending upon the annealing temperature. However, the materials processed by the three different routes show significantly different phase fractions upon annealing, although the phase fractions in the deformed conditions are rather similar. The phase fractions in the MSCR and TSCR(45°) processed materials are quite similar, while the UCR processed material shows significantly different fractions. This indicates that the equilibrium phase fractions are not attained for the combination of annealing temperature and time due to the differences in transformation kinetics, originating from the differences in the deformed microstructures.

The UCR processed material shows much greater hardness as compared to the MSCR and TSCR(45°) processed material after annealing at 800°C, although the hardness values of the EHEA processed by the three different routes are rather similar in the deformed state. The

remarkable difference in the hardness originates from the novel heterogeneous microstructure [37] [38] of the UCR processed and annealed material. As has been clarified recently, the heterogeneous microstructure of the UCR processed and annealed (800°C/1 h) material is composed of different hardness domains which lead to significant back stress strengthening, resulting in simultaneous enhancement in strength and ductility [22]. At higher annealing temperatures, the heterogeneous microstructure transforms into microduplex structure, quite similar to the EHEA processed by the two other processing routes. This leads to very similar hardness values in the EHEA processed by the three different routes at annealing temperature beyond 800°C.

The recrystallization texture in the L1₂/FCC phase of the EHEA processed by the three different routes following annealing at 800°C is featured by the retention of the respective deformation texture components. Since the grain growth is rather limited at this temperature, the texture is mainly influenced by the nucleation pattern in the three processed material. The retention of deformation texture components after annealing has been interpreted in terms of more homogeneous nucleation or absence of preferential nucleation [12]. The apparent similarities in the formation of texture components indicate similar mechanism. The respective texture components are strengthened at higher annealing temperatures due to grain growth.

The annealing texture of the B2 phase in the UCR processed material shows the usual RD and ND-fiber components. The ND fiber is strengthened, particularly after annealing at higher temperatures, as expected for the recrystallization texture of BCC materials. Development of strong ND-fiber is observed even in MSCR and TSCR(45°) processed materials, particularly at higher annealing temperatures. Thus, formation of ND-fiber is preferred irrespective of the processing routes. The presence of strong ND-fiber in the recrystallization texture of BCC materials is usually attributed to greater stored energy of the former [39]. It appears that this mechanism is also responsible for very similar recrystallization texture in the B2 phase dominated by ND-fiber, even though the deformation texture may show characteristic differences [40].

Chapter 6

SUMMARY AND CONCLUSIONS

The main conclusions that may be drawn from the present work are as follows:

1. The UCR processed materials show retention of lamellar regions as opposed completely fragmented microstructure in the MSCR and TSCR(45°) processed material.
2. The development of the B_s^{ND} component in the L12/FCC phase of the MSCR processed material agrees quite well with the texture of cross-rolled single phase FCC materials. However, the texture of the L12/FCC phase in the TSCR(45°) processed material shows significant differences, indicating fundamental differences in deformation pattern.
3. The texture of the B2 phase in the MSCR processed material shows a distinct $\{001\}\langle 110\rangle$ component, which is in good agreement with cross-rolled texture of single phase BCC materials. In the TSCR(45°) material, the texture of the B2 phase is much weaker.
4. Annealing of the UCR processed material at 800 °C results in a remarkably heterogeneous microstructure as opposed to rather homogenous microduplex structure of the MSCR and TSCR(45°) processed materials. However, following annealing at 1000 °C and 1200 °C, the EHEA processed by the three different routes show very similar duplex structure.
5. The heterogeneous microstructure of the UCR processed material results in much greater hardness as compared to the MSCR and TSCR(45°) processed materials annealed at the same temperature of 800 °C for 1 h. The materials processed by the three different routes shows no significant difference in hardness after annealing at 1000 °C and 1200 °C, concomitant with the transformation of the heterogeneous structure of the UCR processed material into duplex structure.

6. The annealing texture of the L12/FCC phase shows presence of α -fiber components and is featured by the retention of the respective deformation texture components. The B2 phase shows strong ND fiber texture, which is the usual recrystallization texture of the BCC materials.

REFERENCES

1. Yeh, J.W., et al., *Nanostructured high-entropy alloys with multiple principal elements: novel alloy design concepts and outcomes*. *Advanced Engineering Materials*, 2004. **6**(5): p. 299-303.
2. Cantor, B., et al., *Microstructural development in equiatomic multicomponent alloys*. *Materials Science and Engineering: A*, 2004. **375-377**: p. 213-218.
3. Senkov, O.N., et al., *Refractory high-entropy alloys*. *Intermetallics*, 2010. **18**(9): p. 1758-1765.
4. Wani, I.S., et al., *Evolution of microstructure and texture during thermo-mechanical processing of a two phase Al_{0.5}CoCrFeMnNi high entropy alloy*. *Materials Characterization*, 2016. **118**: p. 417-424.
5. Zhao, Y.J., et al., *A hexagonal close-packed high-entropy alloy: The effect of entropy*. *Materials & Design*, 2016. **96**: p. 10-15.
6. Zhang, Y., et al., *Microstructures and properties of high-entropy alloys*. *Progress in Materials Science*, 2014. **61**: p. 1-93.
7. Yeh, J.-W., *Alloy design strategies and future trends in high-entropy alloys*. *Jom*, 2013. **65**(12): p. 1759-1771.
8. Yeh, J.W., *Recent progress in high-entropy alloys*. *Annales De Chimie-Science Des Materiaux*, 2006. **31**(6): p. 633-648.
9. Murty, B.S., J.-W. Yeh, and S. Ranganathan, *High-entropy alloys*. 2014: Butterworth-Heinemann.
10. Wani, I.S., et al., *Ultrafine-Grained AlCoCrFeNi_{2.1} Eutectic High-Entropy Alloy*. *Materials Research Letters*, 2016. **4**(3): p. 174-179.
11. Bhattacharjee, P.P., et al., *Evolution of microstructure and texture during warm rolling of a duplex steel*. *Metallurgical and Materials Transactions A*, 2014. **45**(4): p. 2180-2191.
12. Bhattacharjee, P., et al., *Microstructure and texture evolution during annealing of equiatomic CoCrFeMnNi high-entropy alloy*. *Journal of Alloys and Compounds*, 2014. **587**: p. 544-552.
13. Sathiaraj, G.D. and P.P. Bhattacharjee, *Effect of starting grain size on the evolution of microstructure and texture during thermo-mechanical processing of CoCrFeMnNi high entropy alloy*. *Journal of Alloys and Compounds*, 2015. **647**: p. 82-96.

14. Sathiaraj, G.D., et al., *Effect of heavy cryo-rolling on the evolution of microstructure and texture during annealing of equiatomic CoCrFeMnNi high entropy alloy*. Intermetallics, 2016. **69**: p. 1-9.
15. Sathiaraj, G.D., et al., *The effect of heating rate on microstructure and texture formation during annealing of heavily cold-rolled equiatomic CoCrFeMnNi high entropy alloy*. Journal of Alloys and Compounds, 2016. **688**: p. 752-761.
16. Lu, Y., et al., *A Promising New Class of High-Temperature Alloys: Eutectic High-Entropy Alloys*. Scientific Reports, 2014. **4**: p. 6200.
17. Wani, I.S., et al., *Tailoring nanostructures and mechanical properties of AlCoCrFeNi_{2.1} eutectic high entropy alloy using thermo-mechanical processing*. Materials Science and Engineering a-Structural Materials Properties Microstructure and Processing, 2016. **675**: p. 99-109.
18. Lu, Y., et al., *Directly cast bulk eutectic and near-eutectic high entropy alloys with balanced strength and ductility in a wide temperature range*. Acta Materialia, 2017. **124**: p. 143-150.
19. Wani, I.S., et al., *Tailoring nanostructures and mechanical properties of AlCoCrFeNi_{2.1} eutectic high entropy alloy using thermo-mechanical processing*. Materials Science and Engineering: A, 2016. **675**(Supplement C): p. 99-109.
20. Wani, I.S., et al. *Effect of severe cold-rolling and annealing on microstructure and mechanical properties of AlCoCrFeNi_{2.1} eutectic high entropy alloy*. 2017. Institute of Physics Publishing.
21. Wani, I.S., et al., *Cold-rolling and recrystallization textures of a nano-lamellar AlCoCrFeNi_{2.1} eutectic high entropy alloy*. Intermetallics, 2017. **84**: p. 42-51.
22. Bhattacharjee, T., et al., *Simultaneous Strength-Ductility Enhancement of a Nano-Lamellar AlCoCrFeNi_{2.1} Eutectic High Entropy Alloy by Cryo-Rolling and Annealing*. Scientific Reports, 2018. **8**(1): p. 3276.
23. Gurao, N., S. Sethuraman, and S. Suwas, *Effect of strain path change on the evolution of texture and microstructure during rolling of copper and nickel*. Materials Science and Engineering: A, 2011. **528**(25): p. 7739-7750.
24. Suwas, S., et al., *Effect of modes of rolling on evolution of the texture in pure copper and some copper-base alloys*. Zeitschrift für Metallkunde, 2002. **93**(9): p. 918-927.

25. Bhattacharjee, P., S. Saha, and J. Gatti, *Effect of Change in Strain Path During Cold Rolling on the Evolution of Microstructure and Texture in Al and Al-2.5% Mg*. Journal of materials engineering and performance, 2014. **23**(2): p. 458-468.
26. Reddy, S., et al., *Effect of strain path on microstructure and texture formation in cold-rolled and annealed FCC equiatomic CoCrFeMnNi high entropy alloy*. Intermetallics, 2017. **87**: p. 94-103.
27. Gurao, N.P., S. Sethuraman, and S. Suwas, *Evolution of Texture and Microstructure in Commercially Pure Titanium with Change in Strain Path During Rolling*. Metallurgical and Materials Transactions A, 2012. **44**(3): p. 1497-1507.
28. Liu, Y.H., et al., *Strain path dependence of microstructure and annealing behavior in high purity tantalum*. Materials Science and Engineering: A, 2017. **707**: p. 518-530.
29. Stepanov, N., et al., *Effect of cryo-deformation on structure and properties of CoCrFeNiMn high-entropy alloy*. Intermetallics, 2015. **59**: p. 8-17.
30. Zharebtsov, S.V., et al., *Formation of nanostructures in commercial-purity titanium via cryorolling*. Acta Materialia, 2013. **61**(4): p. 1167-1178.
31. Schneider, C.A., W.S. Rasband, and K.W. Eliceiri, *NIH Image to ImageJ: 25 years of image analysis*. Nature methods, 2012. **9**(7): p. 671.
32. Savoie, J. and J.J. Jonas, *Simulation of the deformation textures induced by deep drawing in extra low carbon steel sheets*. Acta Metallurgica Et Materialia, 1994. **42**(12): p. 4101-4116.
33. Toth, L.S., et al., *Development of Ferrite Rolling Textures in Low-Carbon and Extra Low-Carbon Steels*. Metallurgical Transactions a-Physical Metallurgy and Materials Science, 1990. **21**(11): p. 2985-3000.
34. Hong, S.-H. and D.N. Lee, *Deformation and recrystallization textures in cross-rolled copper sheet*. Journal of engineering materials and technology, 2002. **124**(1): p. 13-22.
35. Ostafin, M., J. Pospiech, and R.A. Schwarzer, *Microstructure and Texture in Copper Sheets after Reverse and Cross Rolling*. Solid State Phenomena, 2005. **105**: p. 309-314.
36. Zaid, M. and P. Bhattacharjee, *Electron backscatter diffraction study of deformation and recrystallization textures of individual phases in a cross-rolled duplex steel*. Materials Characterization, 2014. **96**: p. 263-272.
37. Wu, X. and Y. Zhu, *Heterogeneous materials: a new class of materials with unprecedented mechanical properties*. Materials Research Letters, 2017. **5**(8): p. 527-532.

38. Wu, X., et al., *Heterogeneous lamella structure unites ultrafine-grain strength with coarse-grain ductility*. Proc Natl Acad Sci U S A, 2015. **112**(47): p. 14501-5.
39. Rollett, A., et al., *Recrystallization and related annealing phenomena*. 2004: Elsevier.
40. Patel, A., et al., *Strain-path controlled microstructure, texture and hardness evolution in cryo-deformed AlCoCrFeNi 2.1 eutectic high entropy alloy*. Intermetallics, 2018. **97**: p. 12-21.